REFERENCES AND NOTES

1. J. T. Houghton, G. J. Jenkins, J. J. Ephraums, Eds., *Climatic Change: The IPCC Scientific Assessment* (Cambridge Univ. Press, Cambridge, 1990).
2. J. T. Houghton, B. A. Callander, S. K. Varney, Eds., *Climate Change 1992: The Supplementary Report to the IPCC Scientific Assessment* (Cambridge Univ. Press, Cambridge, 1992).
3. R. A. Warrick, E. M. Barrow, T. M. L. Wigley, Eds., *Climate and Sea Level Change: Observations, Projections, and Implications* (Cambridge Univ. Press, Cambridge, 1993).
4. M. F. Meier, *Science* **226**, 1418 (1984).
5. J. A. Church, J. S. Godfrey, D. R. Jacket, T. J. MacDougal, *J. Clim.* **4**, 438 (1991).
6. T. M. L. Wigley, *Geophys. Res. Lett.* **22**, 45 (1995).
7. K. O. Emery and D. G. Aubrey, *Sea Levels, Land Levels, and Tide Gauges* (Springer-Verlag, New York, 1991).
8. A. M. Tushingham and W. R. Peltier, *J. Geophys. Res.* **96**, 4497 (1991).
9. T. P. Barnett, *ibid.* **89**, 7980 (1984).
10. M. Groger and H.-P. Plag, *Global Planet. Change* **8**, 161 (1993).
11. B. C. Douglas, *J. Geophys. Res.* **96**, 6981 (1991).
12. W. R. Peltier and A. M. Tushingham, *Science* **244**, 806 (1989).
13. A. Trupin and J. Wahr, *Geophys. J. Int.* **100**, 441 (1990).
14. G. H. Born, B. D. Tapley, J. C. Ries, R. H. Stewart, *J. Geophys. Res.* **91**, 11775 (1986).
15. B. D. Tapley, C. K. Shum, J. C. Ries, R. Suter, B. E. Schutz, in *Sea Level Changes: Determination and Effects*, P. Woodworth, Ed. (American Geophysical Union, Washington, DC, 1992), vol. 11, pp. 167–180.
16. C. A. Wagner and R. E. Cheney, *J. Geophys. Res.* **97**, 15607 (1992).
17. L.-L. Fu *et al.*, *ibid.* **99**, 24369 (1994).
18. B. D. Tapley *et al.*, *ibid.*, p. 24383.
19. R. S. Nerem *et al.*, *ibid.*, p. 24421.
20. D. A. Imel, *ibid.*, p. 24895.
21. C. S. Ruf, S. J. Keihm, B. Subramanya, M. A. Janssen, *ibid.*, p. 24915.
22. E. J. Christensen *et al.*, *ibid.*, p. 24465.
23. G. T. Mitchum, *ibid.*, p. 24541.
24. R. S. Nerem, E. J. Schrama, C. J. Koblinsky, B. D. Beckley, *ibid.*, p. 24565.
25. The inclusion of the single-frequency altimeter data, which requires the use of an ionosphere correction computed from the DORIS tracking data, did not significantly change the results and thus were included for completeness.
26. E. J. O. Schrama and R. D. Ray, *J. Geophys. Res.* **99**, 24799 (1994).
27. In addition to the removal of data outliers, altimeter data in shallow water (<200 m) and inland seas have been omitted because of tide model uncertainties. Also, a specific location was excluded if the tidally corrected variability of the sea surface was greater than 40 cm rms or if there were less than 40 10-day data points in the time series. The measured global mean sea level variations were insensitive to changes in these criteria.
28. G. S. Hayne, D. W. Hancock, C. L. Purdy, *TOPEX/POSEIDON Research News: JPL 410-42* **3**, 18 (1994).
29. The calibration factor was applied only to the dual-frequency altimeter data; a calibration factor was previously applied to the single-frequency altimeter data by the instrument engineers (*25*).
30. The first 80 days of T/P altimeter data, which are considered anomalous because of spacecraft pointing problems, show a decline of mean sea level of roughly 30 mm that has not been independently verified. However, if these data are included in the analysis presented here, the rate of mean sea level rise over the entire data set is reduced from +3.9 to −1.1 mm/year.
31. W. I. Bertiger *et al.*, *J. Geophys. Res.* **99**, 24449 (1994).
32. A. E. Gill and P. P. Niiler, *Deep-Sea Res.* **20**, 141 (1973).
33. R. W. Reynolds and T. S. Smith, *J. Clim.* **7**, 929 (1994).
34. Global mean SST anomalies were computed by temporally interpolating the weekly 1° by 1° NMC SST fields to the altimeter measurement times, removing the annual and semiannual variations averaged over 1982 to 1994, and then averaging the residuals between ±66° latitude with an equi-area weighting factor.
35. R. W. Reynolds and D. C. Marsico, *J. Clim.* **6**, 115 (1993).
36. Several members of the TOPEX/POSEIDON Science Team have computed a similar rate of sea level rise from the altimeter data, including Minster [J. F. Minster, C. Brossier, P. Rogel, *Eos* **75**, 56 (1994)], Rapp [R. H. Rapp, Y. Yi, Y. M. Wang, *J. Geophys. Res.* **99**, 24657 (1994)], and Wagner [C. A. Wagner *et al.*, *Eos* **75**, 56 (1994)].

38. I thank B. D. Beckley, W. I. Bertiger, P. S. Callahan, E. J. Christensen, L. Fu, B. J. Haines, D. W. Hancock, G. S. Hayne, C. J. Koblinsky, G. Mitchum, K. E. Rachlin, R. H. Rapp, R. D. Ray, E. J. Schrama, and J. Wahr for their comments and contributions. This work was supported by a National Aeronautics and Space Administration TOPEX Project Science Investigation.

27 December 1994; accepted 1 March 1995

Interannual and Interdecadal Variability in 335 Years of Central England Temperatures

G. Plaut, M. Ghil,* R. Vautard

Understanding the natural variability of climate is important for predicting its near-term evolution. Models of the oceans' thermohaline and wind-driven circulation show low-frequency oscillations. Long instrumental records can help validate the oscillatory behavior of these models. Singular spectrum analysis applied to the 335-year-long central England temperature (CET) record has identified climate oscillations with interannual (7- to 8-year) and interdecadal (15- and 25-year) periods, probably related to the North Atlantic's wind-driven and thermohaline circulation, respectively. Statistical prediction of oscillatory variability shows CETs decreasing toward the end of this decade and rising again into the middle of the next.

Low-frequency climate variability, interannual and interdecadal, has been attributed to changes in the oceans' thermohaline circulation (THC) or wind-driven circulation. Multiple equilibria have been found in both THC (*1*) and wind-driven circulation (*2*) models. THC oscillates on scales of decades to millennia (*3*), whereas wind-driven oscillations are seasonal (*4*) or interannual (*5*). The strongest interannual climate signal is associated with the tropical El Niño–Southern Oscillation (ENSO) (*6*). The ENSO does have global effects (*7*), but their details are fairly uncertain at present (*8*). To determine the extent to which extratropical oceanic phenomena or ENSO affect climate variability in the northern mid-latitudes, we examined the CET record (*9*), the longest continuous instrumental temperature record.

Interdecadal and interannual oscillations have been recognized (*10–13*) in global or hemispheric temperature series of shorter duration (*14–16*) by two independent statistical techniques: singular-spectrum analysis (SSA) (*10, 12, 17–19*) and the multitaper method (*11, 20*). Given the shortness of the series, these earlier results are still controversial (*21, 22*). The CET record (*9, 23*) now covers 335 years of averaged monthly temperatures, starting in January 1659 (*24*). Analysis of the CET record should thus settle this controversy, help determine the plausible causes of the peaks that have been detected, and permit a first glimpse at the secular variations of interdecadal variability.

To facilitate comparison with global and hemispheric analyses (*10–13, 20–22*), we performed SSA on the yearly averages of the CET record (*23, 25*). High-frequency interannual variability, such as a quasi-biennial oscillation (*26*), stands out when the monthly, rather than annual, CET data are analyzed with a wide enough SSA window (not shown); this variability is often related to ENSO (*6, 27*). We concentrate here on periods of 5 years and longer; use of a 1-year sampling interval and $M = 40$ lags (*17*) permits the study of periods between 5 and 40 years (*19*). Resolution increases with M, whereas statistical significance decreases. Window widths between 30 and 60 years gave similar results.

A break appears in the singular-spectrum slope (Fig. 1A) at order $k = 11$. A nonparametric Monte Carlo significance test (*19*) confirmed that the record's statistical dimension is $S = 11$ (*28*). The first two empirical orthogonal functions (EOFs) (Fig. 1B) are a data-adaptive running mean and its antisymmetric counterpart (*10, 27*). Eigenvalues 3 to 11 form four pairs (skip-

G. Plaut, Institut Non-Linéaire de Nice, 1361 route des Lucioles, F-06560 Valbonne, France.
M. Ghil, Department of Atmospheric Sciences and Institute of Geophysics and Planetary Physics, University of California, Los Angeles, CA 90095, USA.
R. Vautard, Laboratoire de Météorologie Dynamique du Centre National de la Recherche Scientifique, Ecole Normale Supérieure, 24 rue Lhomond, F-75231 Paris Cedex 5, France.

*To whom correspondence should be addressed.

ping $k = 9$), with the associated EOFs (Fig. 1, B and C) in quadrature. A bidecadal oscillation dominates, because EOFs 3 and 4 have a period T of 25.0 years (Fig. 2). The next pair (EOFs 5 and 6) still corresponds to an interdecadal oscillation: Its spectral density peaks near 14 years. The maximal spectral intensity of EOFs 7 and 8 is at T = 7.7 years, whereas the last pair (EOFs 10 and 11; not shown) has T = 5.2 years. These local CET peaks are in good agreement with the global temperature peaks of (*10*) and with those appearing in the stack spectra (*19*) of the Intergovernmental Panel on Climate Change (IPCC) record (*15*) at 26.3, 14.5, 9.6, 7.5, 5.2, and 4.7 years. The 5- and 15-year oscillations of Mann and Park (*11*) are significant above 90% over Great Britain, whereas the decadal oscillation of Allen and Smith (*12*) is only significant in the tropical Atlantic.

The trend, based on the use of reconstructed components (RCs) (*17*) 1 and 2 (light solid in Fig. 3A), clearly exhibits the 50-year temperature drop of almost 1°C around the year 1700 often associated with the Maunder Minimum (*29*). It also shows that in central England, as in other parts of the Northern Hemisphere (*14, 15, 30*), the most recent warming appeared only in 1985, 10 years later than in the global temperature trend (*10, 14*).

Interdecadal oscillations (heavy solid in Fig. 3A) are based on RCs 3 to 6. They have a peak-to-peak amplitude of over 1°C in some parts of the record, with markedly smaller excursions during the first half of this century; in particular, they contribute very little to CET variability during the first major warming (1910 to 1940). An SSA of the present century's CET, like that of global temperatures in (*21*), produced no bidecadal pair. The bidecadal oscillations (RCs 1 and 2), however, dominate the combined interdecadal and interannual variability (heavy solid in Fig. 3B) in the complete CET record, being strong and fairly regular for more than two centuries. It is hard to imagine that manipulation of the early data alone (*9, 23*) could generate so regular a bidecadal oscillation for over 200 years or lead to a renewed oscillation since 1940.

Interannual oscillations (light solid in Fig. 3B) are dominated by EOF pair 7 and 8. The 8-year period of this pair is longer than any thought to be associated with ENSO (*6, 7, 26, 27, 31*), but periods of 9.1 years (*10*) or of 7.5 and 9.6 years (*19*) also appear in the global temperature records (*14, 15*). EOF pair 7 and 8 is quite robust in the CET record, as it appears with the same periodicity in all subseries of sufficient length. The last significant pair (EOF 10 and 11, not shown), with $T \cong 5$ years, represents in these extratropical temperatures (*7*) the low-frequency component of ENSO (*26, 27, 31, 32*).

The ability of SSA to decompose a time series as a sum of RCs with regular, spectrally band-limited behavior permits the use of low-order, robust autoregressive (AR) models to simulate and forecast each component separately (*19, 31*). We studied the predictability of the CET record by a series of hindcast experiments and then issued a temperature forecast into the next century.

Following the procedure given in (*19*), we performed a series of hindcasts of length 1994 − Y and compared the extrapolated RCs with the true ones; the AR model for the hindcast is based on data up to year Y (*33*) only. The two sets of predicted components we consider are (i) the interdecadal oscillations, EOFs 3 to 6, which have ap-

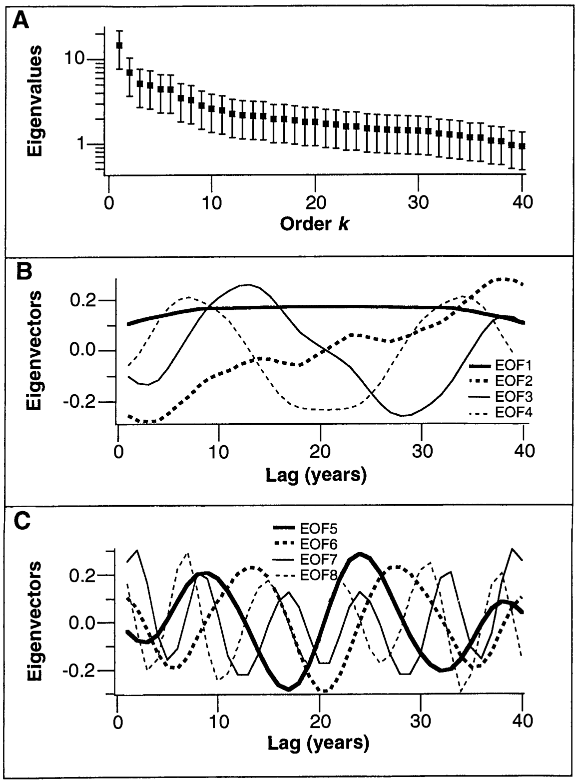

Fig. 1. (**A**) Spectrum of the lag-covariance matrix of the 335-year time series of CET (*9, 23*). Eigenvalues are shown as percentages of the total variance; error bars are from Ghil and Mo (*40*), shown by (*19*) to be conservative. (**B**) The four leading EOFs: The first two represent the local temperature trend and 22% of the variance, The next two the 25-year oscillation and 10% of the variance. (**C**) The next four EOFs: pairs 5 and 6 (peak at 14 years, 9% of variance) and 7 and 8 (8 years, 7%).

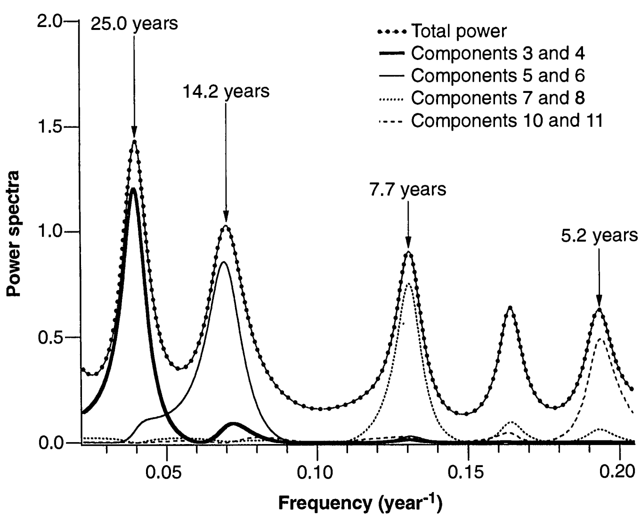

Fig. 2. Stack spectra of the CET record, showing the total power of the temperature time series (dotted line) along with the power in pairs 3 and 4, 5 and 6, 7 and 8, and 10 and 11. A fully consistent spectral approach, combining SSA with the maximum-entropy method (MEM), yields high-resolution spectra with no spurious peaks (*19, 31*). Each PC (*17*), obtained by projecting the record onto an EOF, has a limited harmonic content, allowing the use of low-order MEM. Our results are consistent with those of Folland (*41*), who obtained a 23-year peak by applying high-order MEM to the raw Manley record (*9*). Stocker and Mysak (*39*) found, by the fast Fourier transform, peaks at 24, 15, and 7.4 years, significant at 99%, 98%, and 95%, respectively, against a red-noise process. The spectra of all the PCs sum to the total spectrum (*19*), as apparent from the partial stack in the figure. To form a pair, (i) the difference δf between the spectral peaks of the PCs k and $k + 1$, $\delta f = |f_k - f_{k+1}|$, where f is frequency, has to be small, $\delta f < 3/(8M)$; and (ii) the combined variance of the two PCs, at the frequency f^*, where it is maximum, must exceed 2/3 of the total variance at f^* (*19*). All four pairs in the figure satisfy both criteria (*42*).

proximately the same shape independent of the final year Y, and (ii) the leading set of EOFs, which describes 65% of the total variance or more. The latter set includes nonoscillatory components, and hence, less skill is expected (*19*). We tested our statistical forecast method against two benchmarks (*19*): climatology and persistence. A climatology forecast simply extrapolates the RCs by 0, persistence by their last value. We measure the skill by calculating, for a given lead time τ, the percentage of forecasts that are closer to the true reconstruction than the climatology or persistence (*34*).

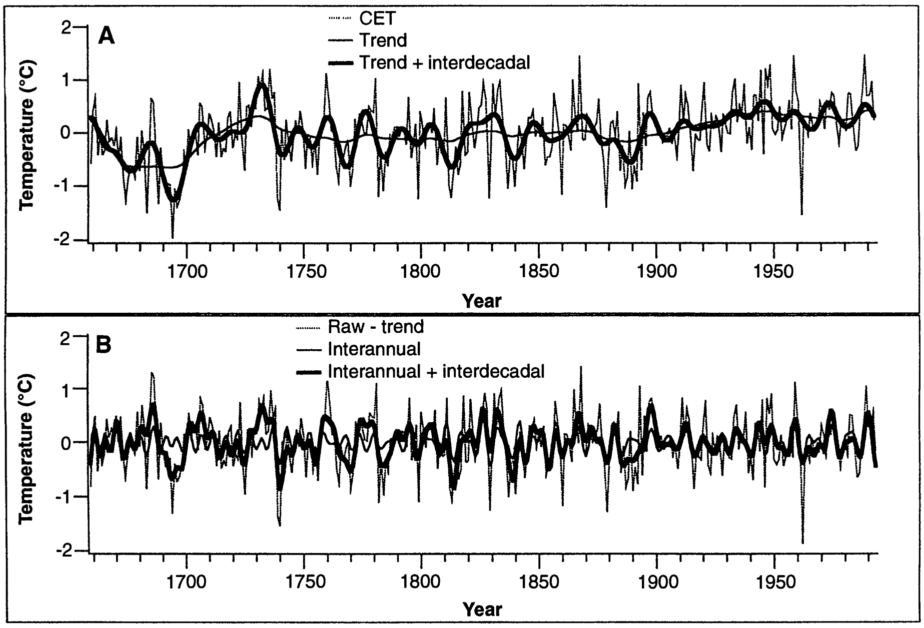

Fig. 3. The RCs of the CET record. RCs provide optimal reconstruction of a dynamic process at precise epochs (*10, 19*). They are not averages over the window width, as the PCs are; as a consequence, the RCs have length N = 335, whereas the PCs have length $N - M + 1$ = 296. Hence, RCs are particularly useful in real-time monitoring and prediction. (**A**) The CET (*23*) time series (dotted curve) together with the reconstructed secular trend (RCs 1 and 2, light solid line) and the trend plus interdecadal oscillations (RCs 1 through 6, heavy solid line); both RCs 3 and 4 (peak at 25 years) and 5 and 6 (peak at 14 years) contribute to the latter. (**B**) The detrended temperature time series (raw data minus RCs 1 and 2, dotted line), the interannual component (RCs 7 and 8 and 10 and 11, light solid line), and the interannual plus interdecadal oscillations (RCs 3 through 8 and 10 and 11, heavy solid line).

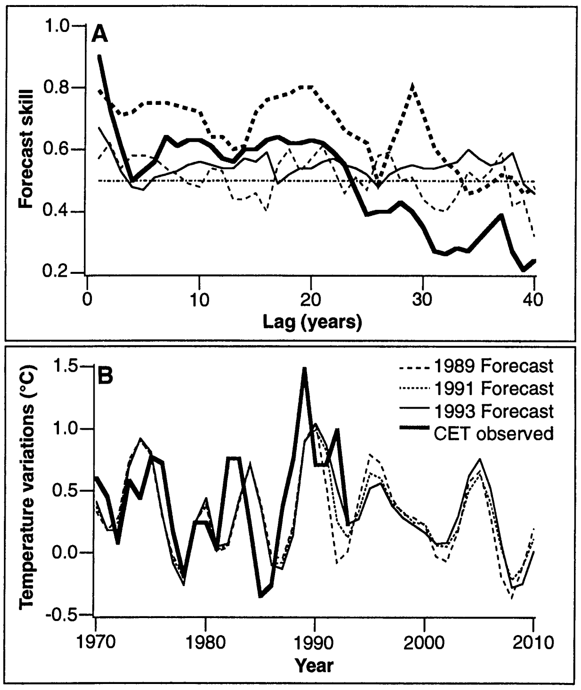

Fig. 4. (**A**) Percentage of AR forecasts that are better than climatology (solid lines) or persistence (dashed lines) for the interdecadal oscillations (EOFs 3 through 6: heavy lines) and for the leading EOFs (65% of the variance or more: light lines). The latter set has, depending on Y, between 11 and 13 EOFs; this number corresponds approximately to the statistical dimension $S(Y)$. (**B**) Leading RC forecasts, after the removal of the time-series average. The raw CET time series (heavy solid line) is shown until February 1993. Three forecasts are illustrated, based on knowledge up to 1989 (dashed line), 1991 (dotted line), and 1993 (light solid line). Cooling for the early part of the decade was already forecast with the 1989 data (in agreement with the Northern Hemisphere forecast of (*10, 12*). All three forecasts indicate that CET is warming for 1994 and 1995, but the warming is less than the record levels attained in 1989 and 1992. Forecasts based on a training set starting in 1722, when the purely instrumental CET record (*23*) begins (not shown), differ from those shown by a slight warming around the year 2000, visible as an inflection point in the figure.

Our forecasts of the interdecadal oscillations are better than climatology up to 24 years ahead, and better than persistence up to 33 years ahead (Fig. 4A). The skill versus climatology drops rapidly at lead times of 1 to 3 years, after which it stays at values of 0.5 to 0.7 for a long time. AR predictability drops faster when all leading components are included: Climatology becomes more skillful at lag 4 and persistence at lag 13. The percentage versus climatology is also between 0.5 and 0.6 after lag 5, indicating that the sign of the anomalies is still forecast correctly more than 50% of the time.

Forecasts of the significant components 1 to 11, which capture over two-thirds of the variability, are in remarkably good agreement with each other, whether we use data up to February 1989, 1991, or 1993 (Fig. 4B, as well as those for 1990, 1992, and 1994, not shown): They all predict a local temperature rise for 1995–1996, a substantial decrease toward the end of the decade, high temperatures in the middle of the next decade, followed by even lower temperatures near 2010. The predicted oscillations exceed by far any local greenhouse warming effect expected by the year 2010 (*15*).

These forecasts concern only stationary climate-system behavior—whether oscillatory, chaotic, or stochastic—and not responses to suddenly or gradually shifting external forcing. Volcanic eruptions do not exhibit any marked regularity over the time interval covered by the CET record, and their main climatic effects seem to disappear in 1 to 2 years (*35*). Thus, the surface-air temperature impact of the Mount Pinatubo eruption in June 1991 is not included in the 1989 prediction of Fig. 4B. According to a general circulation model simulation of the expected impact (*36*), global temperatures for years 1991 to 1993 should have decreased by about 0.3° to 0.5°C, with the maximum impact in late 1992. The local effect of Mount Pinatubo aerosol emissions over England is hard to evaluate from such simulations. If this effect could simply be added to internal climate variability, temperatures should have decreased by about 0.5° to 1°C during these years relative to 1990. The decrease was largest for 1993 and rather less than simple additivity would have suggested. This finding suggests that radiative cooling results from general circulation models should be validated against temperature predictions, as given here and based on internal variability only, rather than against 30-year climatology (36).

To return to plausible causes of the peaks detected in the CET record, the ENSO peak and the quasi-biennial oscillation (26, 27, 31) arise, by and large, in advanced models of the coupled atmosphere-tropical ocean system (6, 37). The interdecadal peak at 15 years and the ENSO peak at 5 years were confirmed by different methods in the instrumental record (11), as well as in a 137-year isotopic proxy record (38). Peaks at 27 and 14 years are present, with 95% significance, in the Koch index of sea-ice extent off Iceland over 370 years (39), and a 17-year peak is present in Philadelphia temperatures over 230 years (39). THC model results emphasizing the North Atlantic should thus contain interdecadal peaks near 15 and 25 years. Likewise, the non-ENSO interannual peak at 7 to 8 years, observed also in U.S. surface-air temperatures (27, 39) and in Atlantic sea level heights (27), should be useful in verifying wind-driven model results for the North Pacific and North Atlantic ocean basins (2, 5).

REFERENCES AND NOTES

1. H. Stommel, *Tellus* **13**, 224 (1961); P. Welander, *Dyn. Atmos. Oceans* **6**, 233 (1982); F. Bryan, *Nature* **323**, 301 (1986); S. Manabe and R. J. Stouffer, *J. Clim.* **1**, 841 (1988); O. Thual and J. C. McWilliams, *Geophys. Astrophys. Fluid Dyn.* **64**, 67 (1992); C. Quon and M. Ghil, *J. Fluid Mech.* **245**, 449 (1992).
2. G. Veronis, *J. Atmos. Sci.* **20**, 577 (1963); S. Y. Chao, *J. Phys. Oceanogr.* **14**, 92 (1984).
3. M. Ghil, A. Mullhaupt, P. Pestiaux, *Clim. Dyn.* **2**, 1 (1987); G. E. Birchfield and W. S. Broecker, *Paleoceanography* **5**, 835 (1990); U. Mikolajewicz and E. Maier-Reimer, *Clim. Dyn.* **4**, 145 (1990); A. J. Weaver, E. S. Sarachik, J. Marotzke, *Nature* **353**, 836 (1991); A. J. Weaver, J. Marotzke, P. F. Cummins, E. S. Sarachik, *J. Phys. Oceanogr.* **23**, 37 (1993); T. Delworth, S. Manabe, R. J. Stouffer, *J. Clim.* **6**, 1993 (1993).
4. B. A. Warren and C. Wunsch, Eds., *Evolution of Physical Oceanography* (MIT Press, Cambridge, MA, 1981); A. R. Robinson, Ed., *Eddies in Marine Science* (Springer-Verlag, New York, 1983).
5. S. J. Auer, *J. Geophys. Res.* **92**, 11709 (1987); M. D. Cox, *J. Phys. Oceanogr.* **17**, 1044 (1987); D. B. Olson, G. P. Podestà, R. H. Evans, O. B. Brown, *Deep-Sea Res.* **35**, 1971 (1988); S. Jiang, F.-f. Jin, M. Ghil, *J. Phys. Oceanogr.*, in press.
6. E. M. Rasmusson and T. H. Carpenter, *Mon. Weather Rev.* **110**, 354 (1982); M. A. Cane, *Science* **222**, 1189 (1983); S. G. H. Philander, *El Niño, La Niña, and the Southern Oscillation* (Academic Press, San Diego, CA, 1990); F.-F. Jin, J. D. Neelin, M. Ghil, *Science* **264**, 70 (1994).
7. E. M. Rasmusson and J. M. Wallace, *Science* **222**, 1195 (1983); C. F. Ropelewski and M. S. Halpert, *Mon. Weather Rev.* **115**, 1606 (1987); P. D. Jones, *Clim. Monit.* **17**, 80 (1989); Y. H. Pan and A. H. Oort, *Clim. Dyn.* **4**, 191 (1990); M. S. Halpert and C. F. Ropelewski, *J. Clim.* **5**, 577 (1992).
8. J. Namias and D. Cayan, *Oceanus* **27** (no. 2), 40 (1984); K. C. Mo, J. Zimmerman, E. Kalnay, M. Kanamitsu, *Mon. Weather Rev.* **119**, 2771 (1991).
9. G. Manley, *Q. J. R. Meteorol. Soc.* **79**, 242 (1953); *ibid.* **100**, 389 (1974).
10. M. Ghil and R. Vautard, *Nature* **350**, 324 (1991).
11. M. E. Mann and J. Park, *Geophys. Res. Lett.* **20**, 1055 (1993).
12. M. R. Allen and L. A. Smith, *ibid.* **21**, 883 (1994).
13. The variable trend in (*10, 14*) was reinterpreted by M. E. Schlesinger and N. Ramankutty [*Nature* **367**, 723 (1994)] as a 65- to 70-year oscillation superimposed on a linear trend.
14. P. D. Jones, T. M. L. Wigley, P. B. Wright, *Nature* **322**, 430 (1986).
15. J. T. Houghton, G. J. Jenkins, J. T. Ephraums, Eds., *Climate Change: The IPCC Scientific Assessment* (Cambridge Univ. Press, London, 1990).
16. J. Hansen and S. Lebedeff, *J. Geophys. Res.* **92**, 13345 (1987); *Geophys. Res. Lett.* **15**, 323 (1988); G. V. Gruza, E. Ya. Ran'kova, E. V. Rocheva, *Meteorol. Gidrol.* **1988**, 16 (1988).
17. SSA is based on eigenvalue-eigenvector decomposition of a time series' lag-covariance matrix (*18*). Given a series of length N and a maximum lag M, the eigenvectors are data-adaptive basis functions and are called EOFs. The eigenvalues are the associated variances λ_k, ordered from largest to smallest. When two eigenvalues are nearly equal and the corresponding, odd and even, EOFs are in phase quadrature, they capture a (nonlinear) oscillation (*19*). SSA can decompose a short, noisy time series into a (variable) trend, periodic oscillations, other statistically significant (but aperiodic) components, and noise. The projection of the time series onto an EOF yields the associated principal component (PC), of length $N - M + 1$. RCs are series of length N that are obtained by the least square fitting of their lagged copies, at lags $0, 1, \ldots M - 1$, to the projection of the original series and its copies onto a given EOF or set of EOFs (*19*).
18. J. M. Colebrook, *Oceanol. Acta* **1**, 9 (1978); D. S. Broomhead and G. P. King, *Physica D* **20**, 217 (1986); K. Fraedrich, *J. Atmos. Sci.* **43**, 419 (1986).
19. R. Vautard and M. Ghil, *Physica D* **35**, 395 (1989); R. Vautard, P. Yiou, M. Ghil, *ibid.* **58**, 95 (1992); M. Dettinger, M. Ghil, C. M. Strong, W. Weibel, P. Yiou, *Eos* **76** (no. 2), 12 (1995).
20. D. J. Thomson, *Proc. IEEE* **70**, 1055 (1982); C. Kuo, C. Lindberg, D. J. Thomson, *Nature* **343**, 709 (1990); P. Yiou *et al.*, *J. Geophys. Res.* **96**, 20365 (1991).
21. J. B. Elsner and A. A. Tsonis, *Nature* **353**, 551 (1991); A. A. Tsonis and J. B. Elsner, *ibid.* **356**, 751 (1992).
22. M. R. Allen, P. L. Read, L. A. Smith, *ibid.* **355**, 686 (1992); *ibid.* **359**, 679 (1992).
23. D. E. Parker, T. P. Legg, C. K. Folland, *A New Daily Central England Temperature Series, 1772–1991* (Tech. Note CRTN11, Hadley Centre, Meteorological Office, Bracknell, Berks, 1991); *Int. J. Climatol.* **12**, 317 (1992).
24. The series was compiled by collecting the diaries of several observers, examining critically the possible differences in observing conditions, and matching the distinct instrumental series during intervals of overlap (*9*). Before 1722, some of these series fail to overlap, so that it was necessary to use noninstrumental weather diaries, the Utrecht time series of A. Labrijn [*Med. Verhandel.* **49**, KNMI No. 102, 1 (1945)], and interpolation (*23*). Hence, the results need to be considered with caution. The series is updated every 3 months in *Weather*.
25. We tried different ways of taking such averages, including a 12-month SSA prefilter (*27*) and 12-month nonoverlapping means starting on different calendar months. All the resulting SSA analyses exhibited similar properties in secular trend, interdecadal oscillations, and interannual oscillations. Starting (*21, 22*) or ending (*19*) the analysis on different years changed the results within reason and as expected from the theory (*19*). We obtained the results shown by using 12-month means beginning on 1 March 1659.
26. E. M. Rasmusson, X.-L. Wang, C. F. Ropelewski, *J. Mar. Syst.* **1**, 71 (1990).
27. M. Dettinger and M. Ghil, in preparation; Y. S. Unal and M. Ghil, *Clim. Dyn.*, in press.
28. The Monte Carlo test (*19*) is based on the simplifying assumption that the analyzed signal is the sum of a deterministic part and of noisy fluctuations, white in time; the latter could result either from measurement errors or from truly stochastic events, such as the climatic perturbations caused by volcanic eruptions (*36*). The statistical dimension S measures the number of significant degrees of freedom, deterministic or stochastic (*10, 19*), in the signal.
29. R. W. Maunder, *Knowledge* **17**, 173 (1894); J. A. Eddy, *Science* **192**, 1189 (1976); E. Nesme-Ribes, *Philos. Trans. R. Soc. London Ser. A* **330**, 487 (1990).
30. P. D. Jones, T. M. L. Wigley, C. K. Folland, D. E. Parker, *Clim. Monit.* **15**, 175 (1987).
31. M. C. Penland, M. Ghil, K. Weickmann, *J. Geophys. Res.* **96**, 22659 (1991); C. L. Keppenne and M. Ghil, *ibid.* **97**, 20449 (1992).
32. A combined SSA analysis of CET and the Southern Oscillation index (*6, 31*), using windows of 15, 20, and 25 years over their 54 years of overlap, exhibits a leading pair with a period of 5 to 6 years, and CET leading the index by ~1 year.
33. We assume that the series is unknown from year Y + 1 to year 2010; Y varies from 1921 to 1994, the hindcast interval. For a given final year Y, SSA with M = 40 yields a set of EOFs. On the basis of these EOFs, a set of PCs (*17*) is built, with a known part of length $Y - (1659 + 39)$ and an unknown part of length $2010 - Y$. An AR model of order 10 is fitted to each PC, with the known part used only as the training interval (*19, 31*). Each PC is extrapolated successively from year $Y, \ldots, Y + t, \ldots$, 1994, on the basis of its own predetermined AR model. The portion of the signal deemed predictable is reconstructed from these extrapolated PCs.
34. For a given lead time $\tau = 2010 - Y$, there are $N_\tau = (73 - \tau)(72 - \tau)/2$ hindcasts but they are not all independent. We based a detailed but still empirical model for their uncertainty on the binomial distribution, with probability P for "success," that is, for exceeding a given forecast (climatology or persistence) in accuracy, and $1 - P$ for failure to do so. The correlation between AR forecasts issued from neighboring initial states is taken into account heuristically to yield $N_\tau' \cong 100$ independent hindcasts. The variance $\sigma(P)$ of the binomial distribution, $\sigma = P(1 - P)$, depends only weakly on P, and we took $\sigma \cong 0.25$. The error bars for Fig. 4A would thus be of the order of $\sigma/\sqrt{N'}$, that is, 0.02 for a 90% confidence level or 0.04 for the 95% level. Another forecasting benchmark is "damped persistence," an order-one AR forecast, in which persistence is damped out over an empirically determined lag to climatology. It was not included explicitly in Fig. 4 to prevent further cluttering and because, given the two benchmarks shown, it cannot outperform the better of the two.
35. J. M. Wallace, in *Natural Climate Variability on Decade-to-Century Time Scales*, D. G. Martinson *et al.*, Eds. (National Academy Press, Washington, DC, in press).
36. J. Hansen, A. Lacis, R. Ruedy, M. Sato, *Geophys. Res. Lett.* **19**, 215 (1992).
37. J. D. Neelin *et al.*, *Clim. Dyn.* **7**, 73 (1992).
38. T. M. Quinn, F. W. Taylor, T. J. Crowley, *Quat. Sci. Rev.* **12**, 407 (1993).
39. T. F. Stocker and L. A. Mysak, *Clim. Change* **20**, 227 (1992).
40. M. Ghil and K. Mo, *J. Atmos. Sci.* **48**, 752 (1991).
41. C. K. Folland, *Meteorol. Mag.* **112**, 163 (1983).
42. SSA-MEM spectra with windows M = 30, 50, and 60 years (not shown; the MEM order is $M - 1$) confirm the peaks in Fig. 2: the peaks at 5.2, 6.2, and 7.7 years do not move at all, the one at 14.2 moves to 12.5 years for M = 30 and to 15 for the two longer windows, whereas the 25-year period can be as long as 28 years. Fourier spectra based on the use of a sliding rectangular or Hanning window [G. M. Jenkins and D. G. Watts, *Spectral Analysis and Its Applications* (Holden-Day, San Francisco, 1968)] of 40 years or longer yield the peaks at 5.2, 7.7, and 14.2 years; a peak near 26 years emerges for window widths equal to or larger than 50 years.

43. We thank M. R. Allen, J. D. Neelin, and P. Yiou for discussions. This work was supported at the University of California, Los Angeles, by the U.S. Department of Energy's National Institute for Global Environmental Change and by a National Science Foundation Special Creativity Award to M.G., and at the Institut Non-Linéaire de Nice and at the Laboratoire de Météorologie Dynamique by the Centre National de la Recherche Scientifique. We thank K. E. Hartman and W. Weibel who helped with the text and figure processing.

19 October 1994; accepted 15 February 1995